FEMS Microbiology Ecology, 93, 2017, fix028

doi: 10.1093/femsec/fix028
Advance Access Publication Date: 0 2017
Research Article

RESEARCH ARTICLE

Organismal and spatial partitioning of energy and macronutrient transformations within a hypersaline mat

Jennifer M. Mobberley[1], Stephen R. Lindemann[2,3], Hans C. Bernstein[1,4], James J. Moran[5], Ryan S. Renslow[1,4], Jerome Babauta[4], Dehong Hu[6], Haluk Beyenal[4] and William C. Nelson[1,*]

[1]Biological Science Division, Earth and Environmental Science Directorate, Pacific Northwest National Laboratory, Richland, WA 99352, USA, [2]Whistler Center for Carbohydrate Research, Department of Food Science, Purdue University, West Lafayette, IN 47907, USA, [3]Department of Nutrition Science, Purdue University, West Lafayette, IN 47907, USA, [4]The Gene and Linda Voiland School of Chemical Engineering and Bioengineering, Washington State University, Pullman, WA 99164, USA, [5]Chemical and Biological Signature Sciences, National Security Directorate, Pacific Northwest National Laboratory, Richland, WA 99352, USA and [6]Environmental Molecular Sciences Laboratory, Earth and Environmental Science Directorate, Pacific Northwest National Laboratory, Richland, WA 99352, USA

*Corresponding author: Pacific Northwest National Laboratory, 902 Battelle Boulevard, P.O. Box 999, MSIN J4-18, Richland, WA 99352, USA, Tel: +509-375-4442; Fax: +509-371-6946; E-mail: William.Nelson@pnnl.gov

One sentence summary: Depth-resolved genome profiling of a microbial mat community from a magnesium-sulfate enriched hypersaline lake reveals metabolic linkages within and between organisms across physiochemical gradients.

Editor: Gary King

ABSTRACT

Phototrophic mat communities are model ecosystems for studying energy cycling and elemental transformations because complete biogeochemical cycles occur over millimeter-to-centimeter scales. Characterization of energy and nutrient capture within hypersaline phototrophic mats has focused on specific processes and organisms; however, little is known about community-wide distribution of and linkages between these processes. To investigate energy and macronutrient capture and flow through a structured community, the spatial and organismal distribution of metabolic functions within a compact hypersaline mat community from Hot Lake have been broadly elucidated through species-resolved metagenomics and geochemical, microbial diversity and metabolic gradient measurements. Draft reconstructed genomes of 34 abundant organisms revealed three dominant cyanobacterial populations differentially distributed across the top layers of the mat suggesting niche separation along light and oxygen gradients. Many organisms contained diverse functional profiles, allowing for metabolic response to changing conditions within the mat. Organisms with partial nitrogen and sulfur metabolisms were widespread indicating dependence on metabolite exchange. In addition, changes in community spatial

Received: 31 October 2016; **Accepted:** 13 March 2017

structure were observed over the diel. These results indicate that organisms within the mat community have adapted to the temporally dynamic environmental gradients in this hypersaline mat through metabolic flexibility and fluid syntrophic interactions, including shifts in spatial arrangements.

Keywords: reconstructed genomes; metagenomics; hypersaline; magnesium sulfate; element transformations; phototrophic

INTRODUCTION

Phototrophic mat communities are compact ecosystems where complete energy and element transformations occur on submillimeter scales (Des Marais 2003; Visscher and Stolz 2005). Capture and recycling of light energy and transformation of nutrients within mat systems result in spatial and temporal biogeochemical gradients (Burow *et al.* 2013; Mobberley *et al.* 2015). Hypersaline mats are ideal systems for studying these energy transformations and cycles as these systems experience low disturbance and often span large oxygen and redox gradients (Des Marais 2003; Harris *et al.* 2013). Despite the high salinities, these ecosystems contain highly diverse microbial communities with populations of oxygenic photoautotrophs localized in the upper, photic zones and a complex consortium of lithoautotrophs, anoxygenic photoautotrophs and heterotrophic consumers deeper in the mat (Bernstein *et al.* 2016; Ley *et al.* 2006; Lindemann *et al.* 2013; Wong *et al.* 2015). In representative non-hypersaline mat systems (e.g. Elkhorn Slough and Octopus Springs), the functional capacity and gene expression of the most abundant community members have been investigated using metagenomics, genome reconstructions and transcriptomics (Burow *et al.* 2014; Klatt *et al.* 2013). However, most investigations of biogeochemical cycles in hypersaline microbial mat systems have focused only on specific processes within carbon, nitrogen and sulfur cycles using functional gene surveys, stable isotope labeling and other biomarkers to examine specific populations and interactions within a community (de Wit, Falcon and Charpy-Roubaud 2005; Finke *et al.* 2013; Houghton *et al.* 2014; Orphan *et al.* 2008). Previous metagenomic studies of hypersaline mats have focused on the overall community-level functional capacity in these systems but have not used genome reconstructions to examine the functional potential of individual organisms within the community across energy and multiple elemental cycles (Kunin *et al.* 2008; Ruvindy *et al.* 2016; Warden *et al.* 2016). As microbial communities operate through interactions, it is important to understand the metabolic capabilities of specific populations of organisms within communities and principles that govern ecosystem functioning. Organism interactions such as metabolite exchange and electron donor/acceptor coupling contribute to community structure and function (Anantharaman *et al.* 2016; Konopka, Lindemann and Fredrickson 2015). In addition, since most microbial habitats are dynamic it is important to understand the roles of metabolic flexibility through functional redundancy and plasticity, niche complementation and division of labor (Lindemann *et al.* 2016).

Here we present organism- and depth-resolved metabolic capabilities related to energy and element cycling within the microbial mat from Hot Lake, a magnesium-sulfate enriched hypersaline lake in north central Washington (Anderson 1958; Zachara *et al.* 2016). The Hot Lake benthic microbial mat is distinct from the Guerrero Negro and Shark Bay hypersaline systems in that it develops seasonally in a non-marine system (Lindemann *et al.* 2013). Throughout the seasonal cycle, the Hot Lake mat is dominated by filamentous cyanobacteria and contains a depth-stratified and diverse bacterial community (Babauta *et al.* 2014; Bernstein *et al.* 2016; Lindemann *et al.* 2013; Moran *et al.* 2014). The ability of the microbial mat to reside in the high magnesium sulfate concentrations of this environment has implications for the search of life on Mars and other planetary bodies (Kilmer *et al.* 2014; Leshin *et al.* 2013), as well as for high salt industrial applications (Oren 2010).

We applied a multifaceted approach incorporating metagenomic sequencing, 16S rRNA gene amplicons, geochemical measurements and ^{13}C stable isotope probing to learn which factors are contributing to the structure and function of this unique ecosystem. Our results link organism resolved functions with major macronutrient cycles and a continuum of spatially resolved niches described by distinct energy inputs to the mat.

MATERIALS AND METHODS

Sampling and physiochemical measurements

Benthic mat samples were collected on 26 June 2012 at 16:00 PDT (photon flux 490 μmol photons PAR m^{-2} s^{-1}; due to partial cloudiness) and 27 June 2012 at 01:00 PDT (photon flux 0 μmol photons PAR m^{-2} s^{-1}) and at 16:00 PDT (photon flux 1225 μmol photon PAR m^{-2} s^{-1}) from a water depth of 35–40 cm located in northeastern Washington state (USA) (48.97347–119.476322). Three intact mat pieces (~50 cm^2) were collected per time point, placed in sterile petri dishes to maintain spatial orientation of the mat, immersed in 2.3 M sucrose for cryoprotection and immediately frozen on dry ice. Mat collected for microscopy was fixed in the field with 4% paraformaldehyde in lake water and stored at 4°C until analysis (see supplemental materials and methods for details). The water temperature was recorded using a WTW 3400i Multi-Parameter Field Meter (WTW, Inc., College Station, TX, USA). Water samples collected for chemical analysis were stored at 4°C in the field and processed as described by Lindemann *et al.* (2013). Irradiance data were collected at each sampling point using a Li-Cor 185 quantum/radiometer/photometer equipped with a LI-190 quantum sensor (Li-Cor, Lincoln, NE) at the site of collection, and were also recorded from a nearby remote automated weather station as previously described (Lindemann *et al.* 2013). Profiling of microbial mat geochemical and light gradients were taken from mat samples placed in an 2-L open channel reactor and Hot Lake water was pumped from the lake continuously during measurements (Babauta *et al.* 2014). Custom-built fiber optic microprobes were used to measure light penetration and dissolved oxygen concentrations (Lewandowski and Beyenal 2013). Carbon accumulation was assessed by lakeside incubation of freshly harvested mat in lake water amended to include 50% [^{13}C] sodium bicarbonate (2.25 mmol added to

740 mL incubation container) as described by Moran et al. (2014). Detailed methodologies for the microelectrode measurements and ^{13}C labeling experiments are in supplemental materials and methods.

Genomic DNA extraction

For cryosectioning, mat subsamples were embedded in Tissue-Tek O.C.T. compound (Electron Microscopy Sciences, Hatfield, PA) and sectioned at 50 μm section depth on a Leica CM1520 cryostat as previously described (Lindemann et al. 2013). Samples were pooled in order to obtain sufficient DNA for each respective sequencing library; for 16S rRNA gene amplicon analysis, subsamples collected on 26 June (01:00 PDT) and 27 June (16:00 PDT) were pooled (250 μm total depth resolution) and for metagenome sequencing subsamples collected on 26 June (16:00 PDT) were combined (1 mm total depth resolution for a total of five metagenome libraries). Genomic DNA from the amplicon (three biological replicates per sample) and metagenome (one biological replicate) cryosections was extracted using an enzymatic protocol as previously described (Lindemann et al. 2013). For the amplicon samples, an additional purification step with the OneStep PCR Inhibitor Removal Kit (Zymo Research, Irvine, CA) was performed. These samples were also amended with 2 $\mu g/\mu l$ of molecular biology grade bovine serum albumin (New England Biosciences, Ipswich, MA) to prevent downstream inhibition.

16S rRNA gene itag sequencing and analysis

Library preparation of the amplicon samples and MiSeq 2×151 was performed by the Argonne National Laboratory NGS Core Facility. The amplification protocol was performed using the broader specificity 515F/806R primer set with each biological replicate amplified in triplicate with unique barcodes (Caporaso et al. 2012; Apprill et al. 2015). Sequences were processed using mothur v1.36 following a pipeline previously described with some modifications (see supplemental materials and methods for commands) (Kozich et al. 2013). A Hot Lake mock community was also included for use in calculating sequencing error rate which was 0.19% (Lindemann et al. 2013). Operational taxonomic units (OTUs) were defined at 97% sequence similarity and classified using the Bayesian classifier against the SILVA reference dataset (Release 123) implemented in mothur. Further characterizations of OTUs to identify closest sequenced 16S rRNA neighbor were performed with the SILVA Incremental Aligner (SINA v1.2.11; Pruesse, Peplies and Glöckner 2012). Alpha diversity metrics were computed in mothur using subsampled sequences (n = 9652). Phyloseq v1.14.0 was used for non-metric multidimensional scaling (NMDS) based Bray-Curtis distance (McMurdie and Holmes 2013). Statistical significance between depth and time was calculated by PERMANOVA testing (999 permutations) using the adonis function in vegan (Oksanen et al. 2013).

Assembly and binning of metagenomes

For the five metagenomes representing each mm of mat, Illumina HiSeq GSIIx paired-end sequencing was performed by the DOE Joint Genome Institute. For each individual library, read quality was initially assessed with FastQC prior to quality trimming with Trimmomatic v0.32 to remove adapter sequences, regions with average quality below 15, and trimmed reads smaller than 36 bp (Andrews 2010; Bolger, Lohse and Usadel 2014). High-quality paired-end reads from each metagenome were assembled individually or combined (coassembly) using IDBA-ud with a minimum contig size of 250 bp (Peng et al. 2012). Short reads were aligned to assembled scaffolds > 1 kb using Bowtie2 for coverage calculations (Langmead and Salzberg 2012). Automatic binning of scaffolds 5 kb and greater from the coassembly and downstream curation was performed with GroopM v 0.3.4 (Imelfort et al. 2014). Gene calling using Prodigal (metagenomic mode) was performed on all scaffolds > 1kb (Hyatt et al. 2010). Completeness and purity of the genome bins were assessed through counting of 102 conserved single-copy genes (Rinke et al. 2013). In order to assess differential coverage of reads from each metagenome to the combined assembly (scaffolds > 1 kb) and to account for differences in sequencing depth between the libraries, we normalized the data as reads per million per scaffold (RPMS):

$$\mathrm{RPMS}_{\mathrm{scaf}} = \frac{\mathrm{coverage}_{\ \mathrm{scaf}} \times\ 10^6}{\sum \mathrm{coverage}}$$

where

$$\mathrm{coverage}\ = \frac{\sum \mathrm{mapped\ read\ length}}{\mathrm{scaffold\ length}}$$

The coverage value representing average reads per base of scaffold was derived from Bowtie2 mappings for each metagenome read set. All coverage values presented are RPMS.

Annotation of metagenomic scaffolds

Several annotation methods were used for functional and taxonomic predictions of proteins on scaffolds >1 kb. Taxonomic assignments of the genome bins were based on Amphora2 classification (Wu and Scott 2012). Bins were assigned to the highest confidence taxonomic level where 75% of the marker genes in the bin had an average confidence interval above 90. A genome bin was classified as a mixed bin containing multiple organisms if <80% of the marker genes were assigned to the same phylum. GhostKOALA was used to assign proteins a single best-hit KEGG Ontology number (KO) which was then used to assess KEGG metabolic pathways (Kanehisa, Sato and Morishima 2015). Hmmer3 was used for hidden Markov model (HMM) searches against Pfam (v.16; score cutoff > gathering threshold), TIGRFAMs (v.15; score cutoff > noise cutoff), FunGene and dbCAN (v.4) databases (Table S1, Supporting Information)(Finn et al. 2015; Fish et al. 2013; Haft, Selengut and White 2003; Johnson, Eddy and Portugaly 2010; Yin et al. 2012). In order to characterize glycoside hydrolases (GH) that are likely involved in extracellular polysaccharide degradation, we used GH carbohydrate-active enzyme (CAZy) families described previously (Berlemont and Martiny 2015). Ribulose-1, 5-bisphosphate carboxylase (RuBisCo) large subunit genes (types I, II, III) were predicted from the PF00016 model based on alignment to identified RuBisCo genes (Tabita et al. 2007). Taxonomic assignment of putative RuBisCo was made by selecting the top hit from a BLASTP against the RefSeq database. This alignment-based approach was also performed with dissimilatory sulfite reductase genes (*dsrB*) to determine those involved in the classical reductive versus the oxidative pathway (Müller et al. 2015). Statistical analyses of scaffolds >1 kb were performed in R using the base statistics (linear regression and Pearson correlations for RPMS of proxy genes versus depth) and the Hmisc package (Spearman correlations for RPMS proxy genes and biogeochemical parameters).

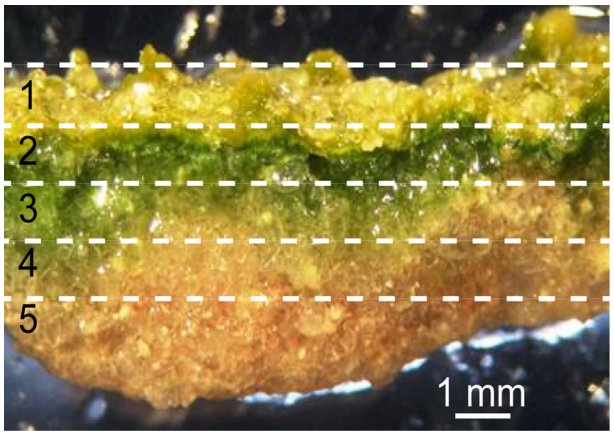

Figure 1. Hot Lake mat morphology. Stereomicroscope image of a cross-section of mat collected on 27 June at 16:00 PST. Dotted lines indicate the approximate sectioning depths. Scale bar = 1 mm. This image was modified with permission from the original version presented in Babauta *et al.* (2014) under the Creative Commons Attribution License.

For single-copy proxy genes in selected biogeochemical cycles, we estimated the percentage of organisms containing the genes per depth by normalizing the RPMS count of a gene on a scaffold by the RPMS of *rpoB*-containing scaffolds detected from all scaffolds 1 kb or greater. The presence of 16S rRNA genes in the coassembly was detected in scaffolds ≥l kb based on SSU HMM models for Archaea, Bacteria and Eukaryota using the SSUfinder script from CheckM (Parks *et al.* 2015). Potential 16S gene fragments were identified from the 250 bp scaffolds by searching the amplicon primers against the sequences using the EMBOSS fuzznuc tool (Rice, Longden and Bleasby 2000). Representative OTU sequences were mapped to all identified 16S rRNA gene fragments from the metagenome scaffolds using NUCmer (Delcher *et al.* 2002). A match was defined as minimum identity >99% across 50–250 bp. Heatmaps were generated in R using pheatmap (Kolde 2015).

Data availability

Sequence data for the metagenomes are publicly accessible in JGI's Integrated Microbial Genomes and Microbiome Samples; Section 1 (3300005974), Section 2 (3300005973), Section 3 (3300005957), Section 4 (3300005976) and Section 5 (3300005965). Raw sequence data for the 16S amplicons are publicly accessible in the NCBI Short Read Archive under project PRJNA326417. Reconstructed draft genome files can be found at https://github.com/jenmobberley/lamMG_assembly.

RESULTS

Light and oxygen gradients in the Hot Lake microbial mat

The benthic phototrophic microbial mat of Hot Lake exists in a magnesium sulfate-dominated hypersaline environment. At the time of sampling, the chemical composition of the Hot Lake water was not carbon deplete (DOC: 9.34 mM C; bicarbonate: 8.62 mM) or sulfate limited (620 mM), but had low concentrations of phosphate (0.56 mM) and dissolved nitrogen compounds were below limit of detection (nitrate: <1.16 mM; nitrite: <0.36 mM) which could potentially influence mat function (Table S2, Supporting Information). The Hot Lake benthic mat sections (thickness between 3–6 mm) displayed three visible layers that formed non-uniform, discrete laminae (Fig. 1).

Total photon flux above mat at time of profiling was 1470 μmol photon PAR m^{-2} s^{-1}. We observed rapid attenuation of wavelengths absorbed by cyanobacterial pigments chlorophyll *a* (440–625 nm) and phycocyanin (625–650 nm) within the top 2 mm of the mat, while there was deeper penetration of wavelengths absorbed by phycoerythrin (560–571 nm) (Fig. 2A). Microscopy based on chlorophyll *a* and phycocyanin autofluorescence showed that filamentous bacteria co-located with the corresponding emission spectra of these pigments and were concentrated just below the surface of the mat (Fig. 2B). Near-infrared (NIR) wavelengths that penetrate deeper into the mat were likely being utilized at depth, as shown by inflection points in the transmission curves at 4 mm, by non-cyanobacterial phototrophs with bacteriochlorophyll *a*-containing photosystems (800–880 nm) (Fig. 2C). Microscopy of a 2.5-mm section of mat showed that bacteriochlorophyll *a* autofluorescence peaked at depths below that of chlorophyll *a* (Fig. 2C).

Physicochemical gradients within the mat were measured at submillimeter increments to profile biogeochemical processes. Dissolved oxygen measured at 16:00 PDT (hereafter termed 'day', incident irradiance 490 μmol photon PAR m^{-2} s^{-1}) was used to calculate profiles of the net photosynthesis rate (see supplementary materials and methods). The net rate increased across the top millimeter of mat then sharply decreased over the next millimeter to suboxia (dissolved oxygen < 1.0 μM) by 3 mm (Fig. 3). All depths measured at 01:00 PDT (termed 'night', incident irradiance 0 $\mu E/m^2/s$) were suboxic (Babauta *et al.* 2014). These measurements identified the location of the oxygen compensation point (~1.1 mm at 490 μmol photons PAR m^{-2} s^{-1}) where the rate of oxygenic photosynthesis is equivalent to the rate of respiration. Stronger incorporation of ^{13}C-labeled bicarbonate occurred within 2 h within the top half of the mat (above the oxygen compensation point) indicating where photoautotrophic primary productivity was prevalent (Fig. S1, Supporting Information). A dark control showed minimal incorporation of ^{13}C label across the mat profile indicating that the experimental result is primarily due to light-induced biological uptake of bicarbonate (data not shown).

Species-resolved genomic data extracted from laminar metagenomes

The oxygen and light microprofiles were used to determine the characteristic length scales that describe specific niches with respect to biological energy availability. This guided sampling of the mat at depth sections that were taken at 1 mm resolution for metagenomic sequencing (Fig. 1). Because of expected overlap in composition between layers, a combined assembly approach (coassembly) of the five metagenome depth sections was taken (Table S3, Supporting Information). From the coassembled metagenome, we recovered 89 genome bins that had at least ×20 average read coverage calculated as reads per million per scaffold (RPMS, see materials and methods) (Table S4, Supporting Information). Conserved single-copy genes analysis indicated 36 bacterial bins were at least 60% complete, with 21 having >90% estimated completeness. The presence of duplicate marker genes and multiple taxonomic assignments in six of the genome bins suggests that these bins contained multiple organisms that could not be resolved due to similar %G+C and coverage values.

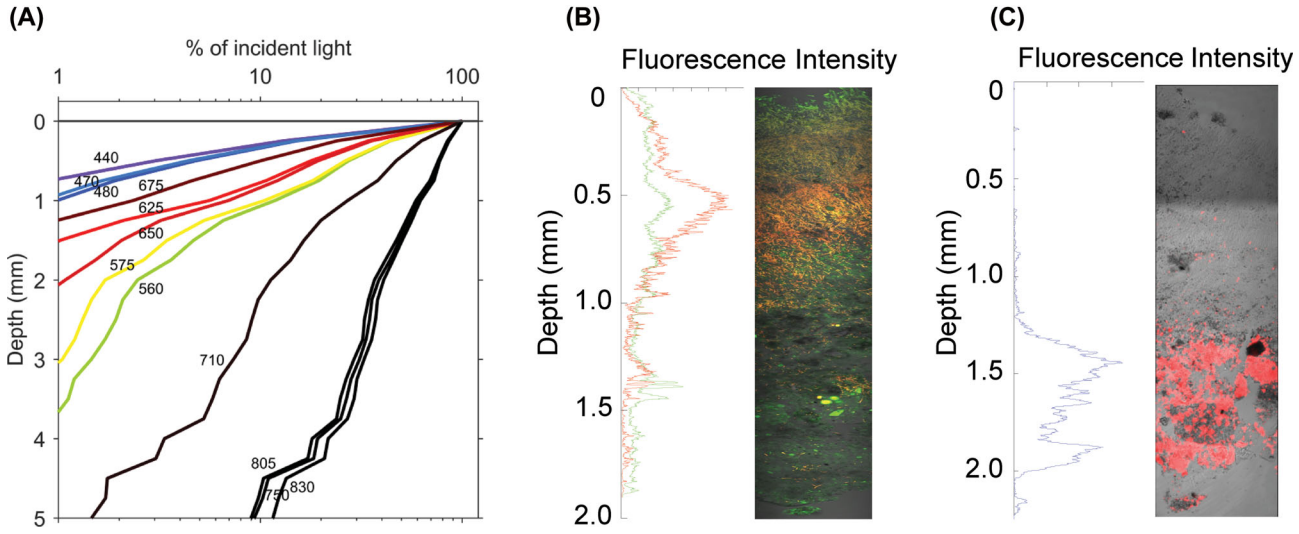

Figure 2. Light microgradients within the Hot Lake microbial mat. (**A**) Attenuation of incident light through the mat measured by a fiber optic microprobe. Values denote wavelength in nanometers. (**B**) Fluorescence image of cyanobacterial pigments in a subsection showing autofluorescence of phycocyanin (red) and chlorophyll *a* (green) overlapping with the bright-field image (gray). The red and green curves are the projections of fluorescence intensities of phycocyanin and chlorophyll *a* to the depth axis, respectively. (**C**) Fluorescence image of bacteriochlorophyll *a* autofluorescence (red) overlapping with the bright-field image (gray). The curve is the projection of the fluorescence intensity to the depth axis.

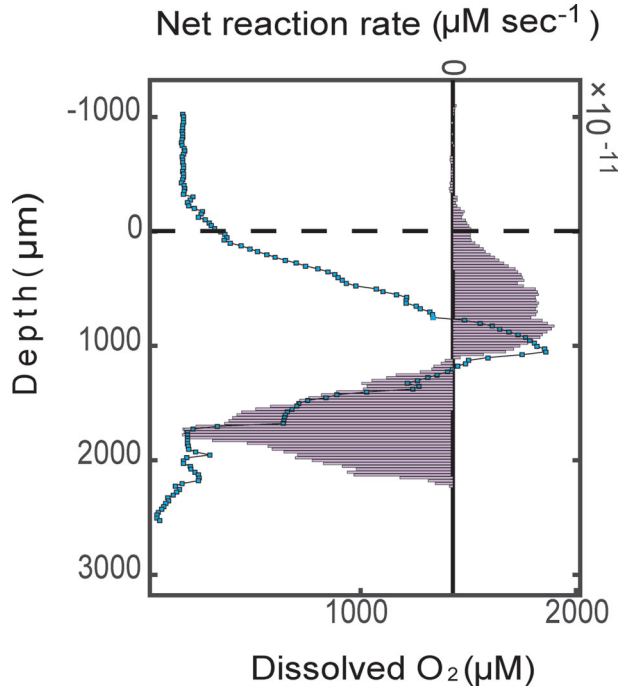

Figure 3. Dissolved oxygen profile and net photosynthesis rate. Dissolved oxygen (blue squares) was measured through the mat profile with a fiber optic microprobe. The net photosynthesis rate (purple bars) was calculated from dissolved oxygen profile and diffusion coefficient (see supplemental methods for calculations). The dotted line indicates the surface of the mat.

This analysis revealed a diverse community of microorganisms differentially distributed within the mat profile (Fig. 4, Table S4). The most abundant, bin HLMG_013, is a likely member of *Leptolyngbya*, and was found to dominate the top 2 mm of the mat. Two other abundant filamentous cyanobacteria, putative members of the order *Oscillatoriales*, HLMG_002 and HLMG_014, had their highest abundances in the second and third mms, respectively. Genome bins similar to *Nanoarchaea* (HLMG_009 and HLMG_086), *Proteobacteria* (HLMG_038 and HLMG_160) and *Melainabacteria* (HLMG_221) were recovered preferentially from the suboxic layers of the mat. Several bacterial genome bins (i.e. HLMG_052 and HLMG_032) were abundant across all layers of the mat.

Functional structure of the mat community

The distribution of different functions was inferred from the presence of genes and pathways in the metagenome. Interestingly, despite strong O_2 and light gradients, many high-level pathways were relatively evenly distributed down the mat's depth (Fig. S2, Supporting Information). The pathways enriched in the top 2 mm were linked to cyanobacterial metabolisms, for instance photosynthetic pigment biosynthesis. Metabolic pathways including carbohydrate transformations and amino acid degradation were enriched within the deep mat (Fig. S2). We tracked the spatial distribution of proxy genes for targeted metabolic pathways involved in energy transformations and acquisition of carbon, nitrogen, sulfur and phosphorus in dominant genomic bins (estimated completeness > 60% or abundance > 40 RPMS, Fig. 4) and in all scaffolds >1 kb (genomic bins and unbinned scaffolds; Fig. 5); all referenced pathways are presented in Table S1. The resulting gene profiles suggest that metabolic flexibility and mixotrophy is a common feature of genomes from the Hot Lake system.

Phototrophy distribution within the Hot Lake microbial mat depth profile

Light availability is one of the primary drivers of biogeochemical cycling within phototrophic mats (Bernstein *et al.* 2016; Des Marais 2003; Lindemann *et al.* 2013). The three most dominant cyanobacteria genomes contained phycocyanin and phycoerythrin light-harvesting pigment genes used in antenna complexes. These genomes also contained type IV-like pilus genes that may be involved in phototaxic twitching and or gliding motility (Khayatan, Meeks and Risser 2015; Wilde and Mullineaux 2015). Non-cyanobacterial genome bins containing genes involved in anoxygenic phototrophy that use NIR light

Draft genome bins

bin	Amphora2 taxonomy	length (bp)	est.compl.
HLMG_013	*Cyanobacteria*	6442193	97%
HLMG_052	*Chloroflexi; Anaerolineae*	3542393	73%
HLMG_011	*Alphaprotobacteria*	2988953	99%
HLMG_044	*Bacteroidetes; Cyclobacterium*	5312747	97%
HLMG_030	*Bacteroidetes;* Candidatus *Amoebophilus*	1313757	65%
HLMG_028	*Planctomycetes; Rhodopirellula*	6120221	94%
HLMG_048	*Proteobacteria**	2115279	61%
HLMG_073	*Bacteria**	3466736	69%
HLMG_049	*Planctomycetes; Planctomycetaceae*	4534718	59%
HLMG_002	*Cyanobacteria*	6389195	96%
HLMG_031	*Planctomycetes; Planctomycetaceae*	4497015	94%
HLMG_033	*Bacteroidetes; Haliscomenobacter*	4454306	87%
HLMG_014	*Cyanobacteria*	3666571	78%
HLMG_162	*Actinobacteria*	3305904	82%
HLMG_032	*Chloroflexi; Anaerolineae*	4189467	82%
HLMG_208	*Gammaproteobacteria*	2813093	86%
HLMG_072	*Deltaproteobacteria; Desulfovibrionales*	2598873	87%
HLMG_196	*Planctomycetes; Planctomycetaceae*	4314315	83%
HLMG_074	*Actinobacteria*	2795384	96%
HLMG_057	*Bacteria* *	3497303	97%
HLMG_207	*Gammproteobacteria; Chromatiaceae*	846096	45%
HLMG_195	*Alphaproteobacteria; Rhodobacteraceae*	2399070	54%
HLMG_214	*Acidobacteria;* Canididatus *Solibacter*	3784578	81%
HLMG_003	*Actinobacteria*	3414963	87%
HLMG_067	*Alphaproteobacteria*	4753382	99%
HLMG_213	*Planctomycetes; Isosphaera*	1995545	42%
HLMG_160	*Alphaproteobacteria; Rhodospirillales*	4693931	97%
HLMG_161	*Bacteria**	2917552	96%
HLMG_200	*Bacteroidetes*	3440783	94%
HLMG_218	*Bacteria*	3103890	96%
HLMG_199	*Bacteroidetes*	1853569	51%
HLMG_038	*Gammaproteobacteria*	4862074	82%
HLMG_040	*Bacteria*	3075467	98%
HLMG_221	*Melainabacteria*	2558797	98%

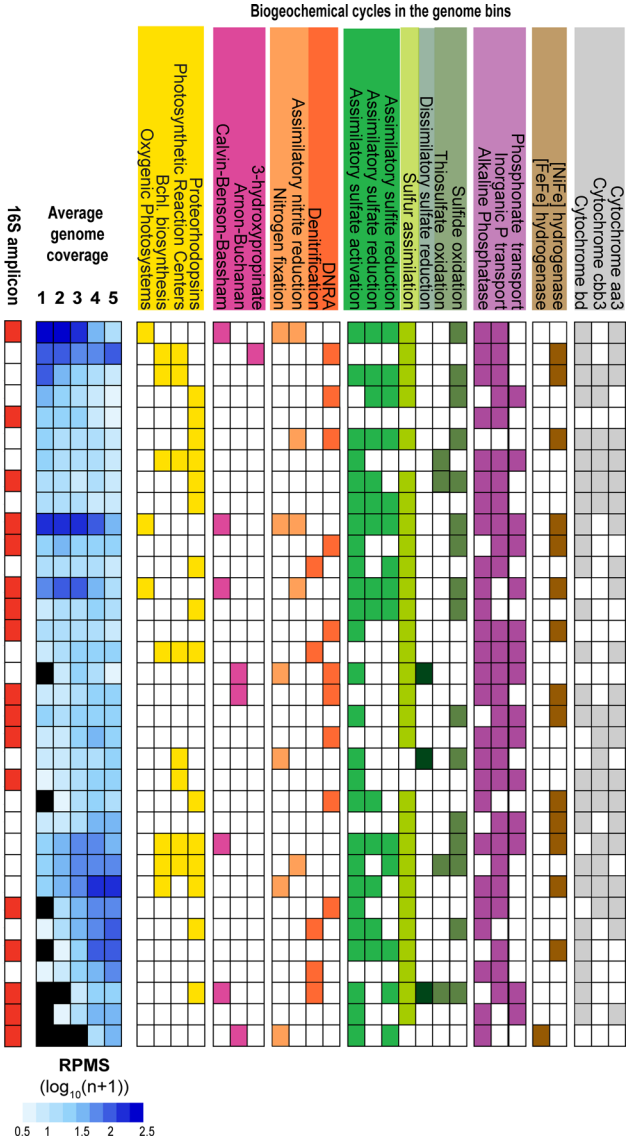

Figure 4. Summary of the major reconstructed genome bins involved in biogeochemical processes. Subset of the 89 reconstructed genome bins that were near complete (>60%) and or had high coverage (> 40 RPMS) containing relevant biogeochemical genes. Taxonomic assignment was based on Amphora2 assignments of marker genes. Genome bins representing multiple phyla are denoted by an asterisk. Average genome coverage is shown as the $\log_{10}(n+1)$ RPMS. Bins with coverage below 1 RPMS in a mat section were omitted. Black fill indicates absence of genome bin in a mat section. Biogeochemical cycles are shown as present (filled) or absent/not detected (white).

(i.e. bacteriochlorophyll synthesis and bacterial photosystems) had more varied depth distribution (Fig. 4, Fig. S3, Supporting Information). In addition to the photosystems, members encoding proteorhodopsins, which harness light to drive an ion gradient for energy generation or membrane transport, peaked in abundance in the 4 mm section (Figs 4 and 5, Fig. S4, Supporting Information).

Distribution of aerobic terminal oxidases and hydrogenases

Like most cyanobacterial mats, oxygen availability showed sharp gradients during the day (Fig. 3) while the mat becomes suboxic at night (Babauta *et al.* 2014). Correspondingly, we observed spatial partitioning of aerobic terminal cytochrome oxidases that are involved in respiration of organic compounds (Fig. 4, Fig. S5, Supporting Information). We observed an increase in the abundance of high-oxygen-affinity cytochromes (*cydAB*, *ccoNOP*), which are used for respiration under reduced oxygen tensions, from non-cyanobacterial organisms with depth (Fig. S3 and S5A, B)(Morris and Schmidt 2013; Stolper, Revsbech and Canfield 2010). Organisms with low-oxygen-affinity cytochromes (*coxA*, *cyoABC*) were also more common at depth (Fig. S5C and D) (Morris and Schmidt 2013). Four genome bins contained no identifiable aerobic terminal cytochrome oxidases.

We also identified hydrogenase genes within 15 of our most complete genome bins (Fig. 4). [NiFe]-Hydrogenases were the most recovered type of hydrogenase suggesting that organisms containing this gene may be involved in oxygen-tolerant hydrogen cycling (Fritsch, Lenz and Friedrich 2013). A single [FeFe]-hydrogenase detected in *Melainabacteria*-like HLMG_221 indicates that this organisms may be producing molecular H_2 as a redox balancing electron sink (Di Rienzi *et al.* 2013).

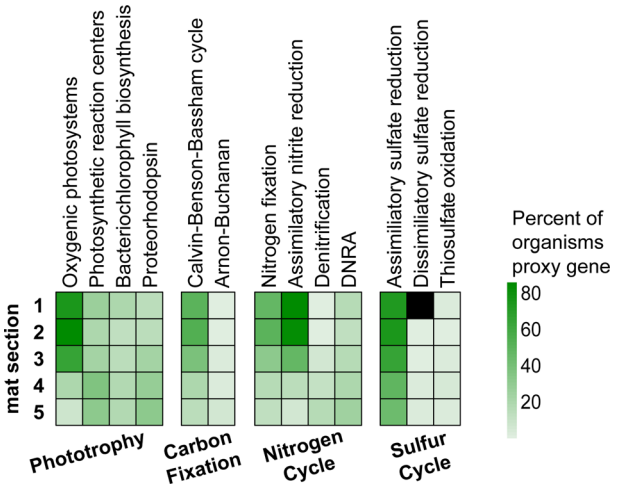

Figure 5. Depth-resolved biogeochemical processes in the Hot Lake metagenome. Summary of selected metabolic processes found in the >1kb greater scaffolds including those found in the genome bins. Relative abundance of the organisms with proxy genes was calculated from the average scaffold coverage values (RPMS) normalized to *rpoB* abundance. Dissimilatory nitrate reduction to ammonia denotes as DNRA. Black fill indicates absence of scaffolds containing proxy genes in a mat section. Genes on scaffolds below 1 RPMS coverage in a mat section were omitted.

Carbon acquisition by the microbial mat

While Hot Lake water has elevated levels of non-humic DOC, likely contributed to by the microbial mat and fauna inputs from the water column, evidence suggests the major route of carbon into the mat is cyanobacterial bicarbonate assimilation (Fig. S1) (Moran *et al.* 2014; Zachara *et al.* 2016). The mat metagenome revealed two dominant carbon fixation pathways: the Calvin-Benson-Bassham reductive pentose phosphate cycle (CBB) and the Arnon-Buchanan cycle (rTCA) (Fig. 5). Ribulose-1, 5-bisphosphate carboxylase (RuBisCo), the primary catalytic enzyme of the CBB cycle, was detected in all three cyanobacterial genomes as well as in non-cyanobacterial genomes that were more abundant at the bottom of the mat (Figs 4 and 6A). Three genome bins (HLMG_072, HLMG_196 and HLMG_221) contained rTCA cycle genes, which showed a strong positive correlation with depth ($r = 0.96$, $P < 0.010$; Fig. S3). The two pathways of carbon fixation were inversely correlated to each other, reflecting the difference in oxygen tension of niches occupied by these species (Fig. S4). In addition, a phototrophic *Chloroflexi*-like organism (HLMG_052) was found to encode genes for the 3-hydroxypropinate cycle (Fuchs Holo; Fig. 4) (Zarzycki *et al.* 2009). We found no evidence of CO dehydrogenase/acetyl-CoA synthase genes within our metagenome indicating that the reductive acetyl-CoA (Wood-Ljungdahl) pathway is not an important component of the major members of the community within the Hot Lake mat.

Carbon fixation and metabolic transformations of fixed carbon contribute to the exopolymeric substance-rich mat matrix of the Hot Lake mat (Fig. 1; Lindemann *et al.* 2013). The Hot Lake microbial mat produces metabolites including osmolytes (e.g. trehalose, glucosylglycerol, gluconate), sugars and polyhydroxyalkanoates which may serve as the primary source of fixed carbon potentially in the form of polysaccharides within the Hot Lake mat (Cole *et al.* 2014). We examined potential polysaccharide catabolism using GH genes as a proxy. The overall representation of polysaccharide-degrading genes was stable across the layers, but there were clear patterns in the organismal distribution of GH genes, both in terms of number of genes and the variety of substrates targeted (Figs S5E and S6, Supporting Information). A majority of the non-cyanobacterial bins with these genes were found to be enriched in the deep mat. Several of the genome bins had high counts of GHs (>1% of genome) with broad predicted polysaccharide substrate range indicating primary roles at biomass degraders (Fig. S6).

Nitrogen cycle partitioning in a nitrogen-limited hypersaline mat

We identified the potential for near-complete cycling of nitrogen within the Hot Lake mat (Fig. 5). At the surface, cyanobacteria were inferred to be the primary conduit for transformation of inorganic nitrogen to organic nitrogen compounds through both the capacity to assimilate dinitrogen and nitrate, although these processes were also identified in other organisms found in the deep mat (Fig. 4 and Fig. S3). For dissimilatory processes, organisms with the capacity to perform anaerobic dissimilatory reduction of nitrate to ammonia (DNRA) were much more abundant than denitrifiers at all depths (Figs 5 and 6B, C). However, genes involved in denitrification, but not DNRA, significantly correlated with depth ($P < 0.050$; Fig. S3). Five of the bacterial genomes that contained genes for incomplete denitrification, either *nirk*/*nirS* or *nosZ*, were most abundant in the 4–5 mm section of the mat (Figs 4 and 6C). There is no clear metagenomic evidence that the mat is capable of aerobic or anaerobic ammonia oxidation as we did not detect ammonia monooxygenase or hydrazine oxidoreductase genes.

Partitioning of the sulfur cycle suggests obligate metabolic exchange

The high concentrations of sulfate within the system may provide a labile sulfur source for the mat community (Table S2). Accordingly, we found sulfate assimilation genes in all depths in the mat (Fig. 5) and across phylogenetically diverse organisms (Fig. 4). Most of the 18 genome bins with partial pathways contained sulfate activation (*cysD2*, *cysN*, *cysNC*/PAPSS) but lacked sulfate reductase genes (*cysH*) and sulfite reduction genes (*cysIJ*, *sir*) (Fig. 4). The seven bins missing assimilatory sulfate reduction genes, except for HLMG_030, contained alternative mechanisms for obtaining sulfur including sulfur transporters, sulfide assimilation genes (*cysM*) and organic sulfur scavenging mechanisms (i.e. sulfatases).

We found that sulfur respiration processes were restricted to a subset of organisms within the community (Figs 4 and 5). Sixteen of the most complete genome bins contained at least one sulfide oxidation gene (*sqr*) and four genome bins contained thiosulfate oxidation (*soxA*) genes (Fig. 4). These genes were distributed throughout all mat depths (Fig. 5) and across a broad range of bacteria with only sulfide oxidation genes in the dominant cyanobacteria correlated to depth ($r = -0.94$, $P < 0.05$; Fig. S3). HLMG_048 and HLMG_073 contained sulfur dehydrogenase genes (*soxCD*) suggesting that complete oxidation of thiosulfate to sulfate occurs in these members, while other organisms contained an incomplete oxidation cycle. Although the overall abundance of dissimilatory sulfate reduction genes (*dsrAB*) was low, these genes were found to be locally abundant in the suboxic mat layers (Fig. 5, Figs S3 and S4). The co-occurrence of *dsrAB* and *aprA* genes in sulfide oxidizers suggests that these two organisms are capable of reverse dissimilatory sulfate reduction to oxidize sulfur and polysulfide to sulfate (Müller *et al.* 2015).

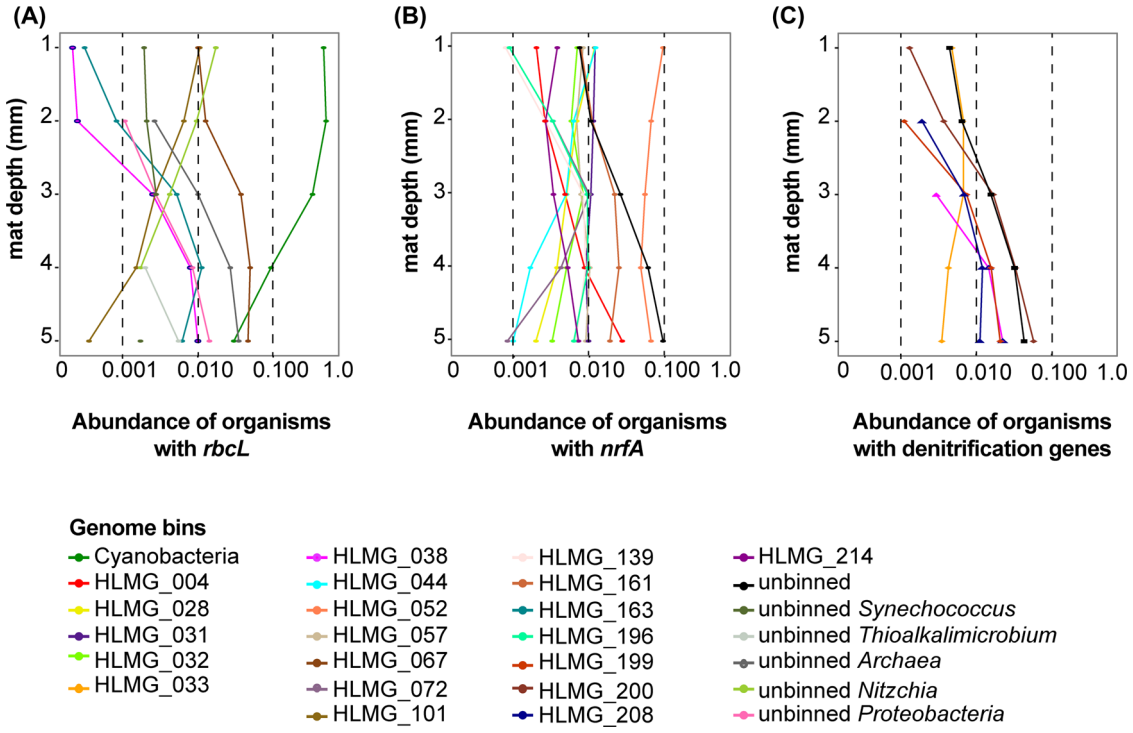

Figure 6. Distribution of genes for carbon fixation and nitrate respiration. (**A**) Depth profile of carbon fixation via the CBB cycle. Proxy gene was ribulose-1,5-bisphosphate carboxylase, large subunit (*rbcL*, PF00016). (**B**) Depth profile of DNRA. Proxy gene was nitrite reductase (*nrfA*). Scaffolds <1 RPMS were omitted. (**C**) Depth profile of denitrification. Proxy genes were Tat-dependent nitrous-oxide reductase (*nosZ*, TIGR04244, diamonds); Sec-dependent nitrous-oxide reductase (*nosZ*, TIGR04246, diamonds); nitrite reductase, cytochrome cd1-containing (*nirS*, Fungenes, triangles); nitrite reductase, copper-containing (*nirK*, TIGR02376, circles).

Extreme phosphorus limitation reflected in the Hot Lake metagenome

Microorganisms within the mat are likely constrained by the availability of organic phosphate due to hypersaline conditions such that the system is reliant upon efficient biomass recycling for phosphate (Cole *et al.* 2014; Lindemann *et al.* 2013). Mechanisms for phosphate salvage and uptake from biomolecules were found to be prevalent at all depths in the mat (Fig. 4, Fig. S5F–J). Twenty-seven of the most complete genome bins contained at least one inorganic phosphate transporter, confirming widespread uptake capacity (Fig. 4, Fig. S5F–H). Alkaline phosphatases from non-cyanobacterial organisms increased in richness with the depth profile (Figs S3 and S5I–J). The presence of phosphonate transporters in 15 of the most complete bins, including two of the dominant cyanobacteria (HLMG_002 and HLMG_014), suggests that these organisms import organic phosphate compounds (Fig. 4). Genes involved in phosphonate biosynthesis (phosphophenolypyruvate mutase and phophonopyruvate decarboxylase) were also recovered, but in low numbers.

Fine-scale taxonomic structure of the mat community

We examined submillimeter-scale community composition related to light regimes with 16S rRNA V4 amplicon sequencing on mat samples collected 27 June 2012 at 16:00 PDT (day) and 01:00 PDT (night). Coverage calculated on normalized sample sets (nseqs = 9652) indicated sufficient sampling (>90% coverage) of the communities (Table S5, Supporting Information). The OTU richness through the depth profile indicated similar richness of the day and night samples but increased stratification within the day profile (Fig. 7 and Table S5). During the day, cyanobacterial relative abundance was greatest in the top 3 mm of the mat with a transition to higher abundances of non-cyanobacterial species including members of *Alphaproteobacteria, Deltaproteobacteria*, including sulfate-reducing bacteria, and *Bacteroidetes* at depth (Fig. 7A). At night, stratification was not apparent, as reads from cyanobacteria were dominant throughout the depth profile (Fig. 7B). Representative sequences of the OTUs mapped to 16S rRNA sequences found within 29 genome bins and 44 unbinned scaffolds at >99% identity (Fig. 4). Together, these mapped OTUs accounted for an average relative abundance of 60% across all samples indicating that both the metagenome and amplicon approaches captured the dominant organisms within the mat community.

The light regime dynamically influenced community structure of the mat. The Bray–Curtis dissimilarity based on the 515 OTUs that composed >0.01% of the total OTUs showed that day and night mat samples were distinct (NMDS stress = 0.091); however, there was within-sample variation at all depths (Fig. 7C). The matched samples indicated that the community structure shifts across depth ($R^2 = 0.36$, $P < 0.002$) and, to a lesser extent, the diel cycle ($R^2 = 0.09$, $P < 0.002$) (Fig. 7C). Furthermore, when considering the OTUs from these samples that mapped to the genome bins, while there were some spatial shifts in the relative abundances within the mat between the day and night samples, the overall depth patterns for most genome bins were consistent (Fig. S7, Supporting Information). During the day, the cyanobacteria and sulfur-oxidizing bacteria displayed peak relative abundances in oxic sections of the mat while others capable of anaerobic respiration were highest in the suboxic sections of the mat.

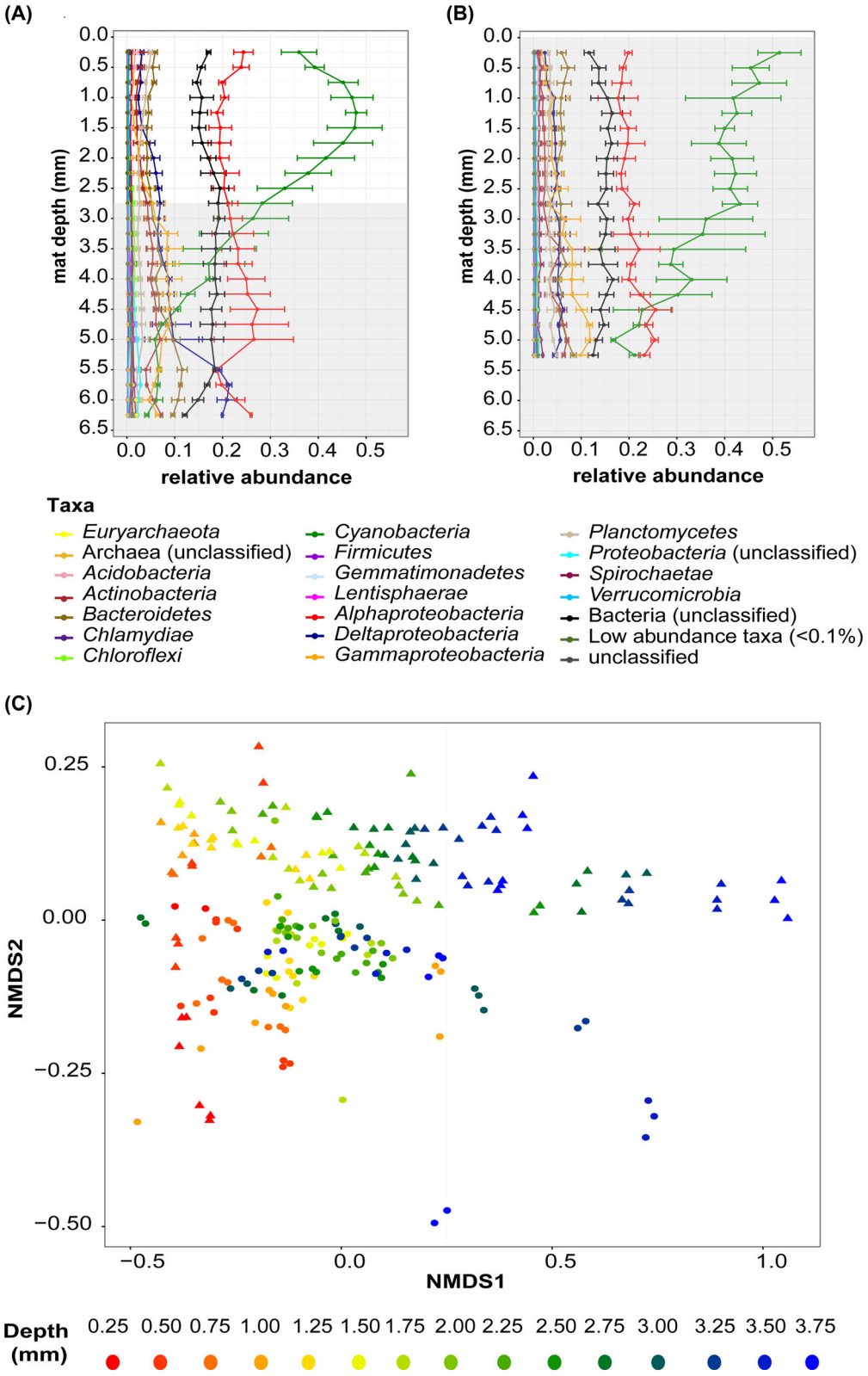

Figure 7. Shifts in community structure occur over the diel. (**A**) Average relative abundance of OTUs (>0.1%) through the depth profile at 16:00 PST. Error bars represent standard deviation. Shaded portion indicates suboxic conditions measured with the microelectrode probe. (**B**) Average relative abundance of OTUs (>0.1%) through depth profile at 01:00 PST. Error bars represent standard deviation. Shaded portion indicates suboxic conditions measured with the microelectrode probe. (**C**) NMDS of OTUs (>0.01%) from day (circles) and night (triangles). Samples depths are represented as gradient color.

DISCUSSION

Cyanobacteria are the primary producers in phototrophic microbial mats, providing captured energy and fixed inorganic macronutrients to the other members of the mat community. The Hot Lake mat is primarily composed of *Leptolyngbya* and *Oscillatoriales* type organisms in contrast to comparable marine and hot spring systems where *Coleofasciculus* (formerly known as *Microcoleus*) and unicellular cyanobacteria are often dominant, respectively (Burow *et al*. 2013; Jonkers *et al*. 2003; Klatt *et al*. 2011; Ley *et al*. 2006; Wong, Ahmed-Cox and Burns 2016). These different cyanobacterial populations likely reflect the unique physiochemical features of the Hot Lake water, such as divalent salinity and high sulfate concentration that have a selective force on the lifestyles of the primary producers in these systems. We observed differential distribution of the three highly abundant cyanobacteria across the sharp daytime light and oxygen gradients observed in the top 3 mm of the mat. We hypothesize that this vertical spatial arrangement reflects their respective phototrophic niches and is likely mediated by light and oxygen tolerances. There was no discernable difference in pigment biosynthesis and photosystem gene content among the cyanobacteria, suggesting that differences in light-harnessing potential result from alternate alleles or regulation of these genes in response to changing environmental stresses such as irradiance or ultraviolet exposure (Gan *et al*. 2014; Yamazaki, Nomata and Fujita 2006). However, there are differences in metabolic potential between the three genomes that could influence spatial partitioning. For example, the draft genome HLMG_013 lacked a bidirectional hydrogenase (*hox*), which may be important for regeneration of reducing equivalents during fermentative growth under suboxic conditions (Hoffmann *et al*. 2015). As HLMG_013 was most abundant in the top mm of the mat, it is less exposed to suboxic conditions. The other two dominant cyanobacteria partition deeper in the mat and may use *hox* to deal with prolonged exposure to suboxic conditions.

Despite differences in cyanobacteria populations, many of the reconstructed bacterial genomes from the Hot Lake mat are taxonomically similar to those found across phototrophic mats. We identified members of *Proteobacteria*, *Chloroflexi*, *Bacteroidetes*, *Actinobacteria* and *Planctomycetes*, all of which were found in other hypersaline mat systems (Wong, Ahmed-Cox and Burns 2016). Based on their genome content, many of these organisms are involved in biomass transformations through phototrophic or heterotrophic growth. We saw an increase in abundance and richness of organisms with biomass recycling pathways such as degradation of amino acids and enzymes including GHs and alkaline phosphatases within the deep mat. These functions indicate that the population in the suboxic mat primarily degrades organic material and biomass. This suggests that, although the Hot Lake primary producers are distinct from other systems, the products provided by those cyanobacteria are similar or the same, and thus the underlying metabolisms, particularly in consuming and recycling of biomass, are conserved.

Non-cyanobacterial organisms were identified that may contribute fixed carbon to the Hot Lake mat under light conditions that preclude cyanobacteria. For example, the broadly and evenly distributed metabolically flexible *Anaerolinea*-like organism (HLMG_052) could exploit the high spatial and temporal heterogeneity in light and oxygen gradients through heterotrophic growth on cyanobacterial-produced photosynthate in the upper portions of the mat while those populations in the deep mat may harness daytime NIR for carbon fixation (Bernstein *et al*. 2016; Finke *et al*. 2013; Klatt *et al*. 2011). Additionally, we also found that organisms capable of phototrophic or chemotrophic carbon fixation were found in the suboxic region of the mat which may contribute to carbon incorporation observed in the deep mat (Fig. S1). This included organisms capable of thiosulfate oxidation and oxidative dissimilatory sulfate reduction (rdsr), which may indicate autotrophic growth through anoxygenic photosynthesis (Friedrich *et al*. 2005). Three other genome bins recovered in the suboxic mat layers contained genes for potential dark carbon fixation through the rTCA cycle (Hug *et al*. 2016). This metabolism co-occurred with anaerobic respiration processes including DNRA, dissimilatory sulfate reduction, and hydrogenases. The absence of methanogens and acetogenic archaea in the Hot Lake mat and presence of nanoarchaeal-like genome bins suggests that archaea are not significantly contributing to carbon fixation, unlike other hypersaline mat systems (López-López *et al*. 2013; Orphan *et al*. 2008; Ruvindy *et al*. 2016). The extent of energy and carbon capture below the photic zone has yet to be determined, but may be important to maintaining community functional stability.

The atypical hypersaline chemistry of Hot Lake appears to shape the distribution of nitrogen respiratory redox pathways within the mat. The sulfate concentration of Hot Lake (620 mM at this sampling) is nearly eight times higher than has been recorded for the Guerrero Negro salterns (Fike *et al*. 2008). The high carbon and sulfur and low nitrate conditions in the system are likely inhibitory to denitrification activity, which could explain our observation of low representation of denitrification genes within the mat profile (Burgin and Hamilton 2007; Yoon *et al*. 2015). No complete denitrification cycle was observed in any of the dominant organisms, providing evidence that this process may be divided across multiple organisms. Additionally, the high carbon and low nitrate conditions in the mat are conditions that are favorable to DNRA which could explain the broader distribution of these genes observed (Strohm *et al*. 2007; Yoon *et al*. 2015). Ammonium excreted by organisms performing DNRA is likely assimilated by other members of the mat consortium instead of being oxidized, as no metagenomic evidence for nitrification or anammox was found. Although genes for archaeal ammonia oxidation have been recovered from marine hypersaline systems, this process may be inhibited by the higher salt concentrations and the high divalent ion concentration, relative to a marine-influenced system, (López-López *et al*. 2013; Oren 2011; Ruvindy *et al*. 2016).

We also observed potential for the oxidative sulfur cycle processes to supply bioavailable sulfide species. Sulfide and incomplete thiosulfate oxidation pathways were found within 15 of the near-complete reconstructed genomes suggesting that these organisms may produce sulfur or polysulfide that other nearby organisms could incorporate into cysteine via *cysM*. These findings indicate the potential connections between assimilatory and dissimilatory pathways that could result from a division of labor of these processes. Similar to DNRA, sulfide oxidation is broadly distributed through organisms across the depth profile. This distribution of function reflects niche partitioning of populations and metabolic flexibility that enables community members to respond to the changing conditions over the diel.

Changes in the spatial arrangement of organisms across the diel cycle suggest broad restructuring of nutrient and element flow paths through the community. The shifts in organismal distribution observed in the 9 h between sampling are likely attributed to cellular migration although over that time scale there may be diel fluctuation in organism population sizes. The variation in cyanobacterial distribution over the diel and the presence of genes implicated in motility suggest that these cyanobacteria

migrate in response to changing light and oxygen gradients over the course of a diel (Garcia-Pichel, Mechling and Castenholz 1994; Kruschel and Castenholz 1998). Thus, we expect that spatial arrangement of cyanobacteria within the mat is dynamic and strongly influences the positions and activities of other members throughout the diel cycle. This suggests that there is wide-scale rewiring of metabolic networks across the diel cycle that alters the flow of energy and element transformations such as fermentation of cyanobacterially produced compounds at night (Lee *et al*. 2014; Stuart *et al*. 2015). Some organisms, particularly those that cannot migrate, might respond through a change in expressed metabolic activity, which could in part explain the observed shallow gene gradients for some energy and macronutrient cycles.

Species-resolved metagenomics with geochemical and metabolic gradient measurements has, for the first time, broadly elucidated the spatial and organismal distribution of metabolic functions that are important to energy and element flow within a compact hypersaline community. When compared to other hypersaline mat systems, the Hot Lake mats contained different dominant cyanobacterial populations but a similar collection of other taxa. Genomic reconstructions revealed that many organisms contained partial cycles for assimilation and respiration of nitrogen and sulfate, as well as alternative carbon fixation pathways suggesting syntrophic interactions and division of labor. We observed widespread metabolic flexibility within the draft genomes indicating that community members are poised to respond to environmental changes that occur over the diel such as light spectra penetration, oxygen concentration and metabolic substrate availability. We observed shifts in spatial arrangements of phototrophic organisms which would lead to a daily cycle of rewiring of linkages between energy and macronutrient transformation. Together our multifaceted approach suggests that the energy and biogeochemical partitioning within hypersaline mats is much more dynamic than previously thought.

SUPPLEMENTARY DATA

Supplementary data are available at *FEMSEC* online.

ACKNOWLEDGEMENTS

The authors would like to thank Heather Engelmann, Sergey Stolyar, Young-Mo Kim, Jim Fredrickson, Roslyn Brown, Alex Cory, and Alice Dohnalkova for sample collection. The authors would also like to acknowledge the U.S. Bureau of Land Management, Wenatchee Field Office, for their assistance in authorizing this research and providing access to the Hot Lake Research Natural Area.

FUNDING

This work was supported by the U.S. Department of Energy (DOE), Office of Biological and Environmental Research (BER), as part of BER's Genomic Science Program (GSP). This contribution originates from the GSP Foundational Scientific Focus Area (FSFA) at the Pacific Northwest National Laboratory (PNNL). A portion of the research was performed using Environmental Molecular Sciences Laboratory (EMSL), a DOE Office of Science User Facility sponsored by the Office of Biological and Environmental Research and located at Pacific Northwest National Laboratory. The Pacific Northwest National Laboratory is operated for DOE by Battelle Memorial Institute under contract DE-AC05-76RL01830. Authors Hans C. Bernstein and Ryan S. Renslow are grateful for support given by the Linus Pauling Distinguished Postdoctoral Program, a Laboratory Directed Research Program of PNNL.

REFERENCES

Anantharaman K, Brown CT, Hug LA *et al*. Thousands of microbial genomes shed light on interconnected biogeochemical processes in an aquifer system. *Nat Commun* 2016;**7**:13219.

Anderson G. Some limnological features of a shallow saline meromictic lake. *Limnol Oceanogr* 1958;**3**:259–70.

Andrews S. FastQC: A quality control tool for high throughput sequence data. Available online at http://www.bioinformatics.babraham.ac.uk/projects/fastqc, 2010.

Apprill A, McNally S, Parsons R *et al*. Minor revision to V4 region SSU rRNA 806R gene primer greatly increases detection of SAR11 bacterioplankton. *Aquatic Microbial Ecology* 2015;**75**:129–37.

Babauta JT, Atci E, Ha PT *et al*. Localized electron transfer rates and microelectrode-based enrichment of microbial communities within a phototrophic microbial mat. *Front Microbiol* 2014;**5**:11. doi:10.3389/fmicb.2014.00011.

Berlemont R, Martiny AC. Genomic potential for polysaccharide deconstruction in bacteria. *Appl Environ Microb* 2015;**81**:1513–9.

Bernstein HC, Brislawn C, Renslow RS *et al*. Trade-offs between microbiome diversity and productivity in a stratified microbial mat. *ISME J* 2016; doi: 10.1038/ismej.2016.133.

Bolger AM, Lohse M, Usadel B. Trimmomatic: a flexible trimmer for Illumina sequence data. *Bioinformatics* 2014;**30**:2114–20.

Burgin AJ, Hamilton SK. Have we overemphasized the role of denitrification in aquatic ecosystems? A review of nitrate removal pathways. *Front Ecol Environ* 2007;**5**:89–96.

Burow L, Woebken D, Marshall I *et al*. Identification of Desulfobacterales as primary hydrogenotrophs in a complex microbial mat community. *Geobiology* 2014;**12**:221–30.

Burow LC, Woebken D, Marshall IP *et al*. Anoxic carbon flux in photosynthetic microbial mats as revealed by metatranscriptomics. *ISME J* 2013;**7**:817–29.

Caporaso JG, Lauber CL, Walters WA *et al*. Ultra-high-throughput microbial community analysis on the Illumina HiSeq and MiSeq platforms. *ISME J* 2012;**6**:1621–4.

Cole JK, Hutchison JR, Renslow RS *et al*. Phototrophic biofilm assembly in microbial-mat-derived unicyanobacterial consortia: model systems for the study of autotroph-heterotroph interactions. *Front Microbiol* 2014;**5**:109. doi: 10.3389/fmicb.2014.00109.

de Wit R, Falcon LI, Charpy-Roubaud C. Heterotrophic dinitrogen fixation (acetylene reduction) in phosphate-fertilised Microcoleus chthonoplastes microbial mat from the hypersaline inland lake 'la Salada de Chiprana'(NE Spain). *Hydrobiologia* 2005;**534**:245–53.

Delcher AL, Phillippy A, Carlton J *et al*. Fast algorithms for large-scale genome alignment and comparison. *Nucleic Acids Res* 2002;**30**:2478–83.

Des Marais DJ. Biogeochemistry of hypersaline microbial mats illustrates the dynamics of modern microbial ecosystems and the early evolution of the biosphere. *Biol Bull* 2003;**204**:160–7.

Di Rienzi SC, Sharon I, Wrighton KC *et al.* The human gut and groundwater harbor non-photosynthetic bacteria belonging to a new candidate phylum sibling to Cyanobacteria. *Elife* 2013;**2**:e01102.

Fike DA, Gammon CL, Ziebis W *et al.* Micron-scale mapping of sulfur cycling across the oxycline of a cyanobacterial mat: a paired nanoSIMS and CARD-FISH approach. *ISME J* 2008;**2**:749–59.

Finke N, Hoehler TM, Polerecky L *et al.* Competition for inorganic carbon between oxygenic and anoxygenic phototrophs in a hypersaline microbial mat, Guerrero Negro, Mexico. *Environ Microbiol* 2013;**15**:1532–50.

Finn RD, Coggill P, Eberhardt RY *et al.* The Pfam protein families database: towards a more sustainable future. *Nucleic Acids Res* 2015;**44**:D279–85.

Fish JA, Chai B, Wang Q *et al.* FunGene: the functional gene pipeline and repository. *Front Microbiol* 2013;**4**:291.

Friedrich CG, Bardischewsky F, Rother D *et al.* Prokaryotic sulfur oxidation. *Curr Opin Microbiol* 2005;**8**:253–9.

Fritsch J, Lenz O, Friedrich B. Structure, function and biosynthesis of O2-tolerant hydrogenases. *Nat Rev Microbiol* 2013;**11**:106–14.

Gan F, Zhang S, Rockwell NC *et al.* Extensive remodeling of a cyanobacterial photosynthetic apparatus in far-red light. *Science* 2014;**345**:1312–7.

Garcia-Pichel F, Mechling M, Castenholz RW. Diel migrations of microorganisms within a benthic, hypersaline mat community. *Appl Environ Microb* 1994;**60**:1500–11.

Haft DH, Selengut JD, White O. The TIGRFAMs database of protein families. *Nucleic Acids Res* 2003;**31**:371–3.

Harris JK, Caporaso JG, Walker JJ *et al.* Phylogenetic stratigraphy in the Guerrero Negro hypersaline microbial mat. *ISME J* 2013;**7**:50–60.

Hoffmann D, Maldonado J, Wojciechowski MF *et al.* Hydrogen export from intertidal cyanobacterial mats: sources, fluxes and the influence of community composition. *Environ Microbiol* 2015;**17**:3738–53.

Houghton J, Fike D, Druschel G *et al.* Spatial variability in photosynthetic and heterotrophic activity drives localized δ13Corg fluctuations and carbonate precipitation in hypersaline microbial mats. *Geobiology* 2014;**12**:557–74.

Hug LA, Thomas BC, Sharon I *et al.* Critical biogeochemical functions in the subsurface are associated with bacteria from new phyla and little studied lineages. *Environ Microbiol* 2016;**18**:159–73.

Hyatt D, Chen G-L, LoCascio PF *et al.* Prodigal: prokaryotic gene recognition and translation initiation site identification. *BMC Bioinformatics* 2010;**11**:1.

Imelfort M, Parks D, Woodcroft BJ *et al.* GroopM: an automated tool for the recovery of population genomes from related metagenomes. *PeerJ* 2014;**2**:e603.

Johnson LS, Eddy SR, Portugaly E. Hidden Markov model speed heuristic and iterative HMM search procedure. *BMC Bioinformatics* 2010;**11**:1.

Jonkers HM, Ludwig R, De Wit R *et al.* Structural and functional analysis of a microbial mat ecosystem from a unique permanent hypersaline inland lake: 'La Salada de Chiprana' (NE Spain). *FEMS Microbiol Ecol* 2003;**44**:175–89.

Kanehisa M, Sato Y, Morishima K. BlastKOALA and GhostKOALA: KEGG tools for functional characterization of genome and metagenome sequences. *J Mol Biol* 2016;**428**:726–31.

Khayatan B, Meeks JC, Risser DD. Evidence that a modified type IV pilus-like system powers gliding motility and polysaccharide secretion in filamentous cyanobacteria. *Mol Microbiol* 2015;**98**:1021–36.

Kilmer BR, Eberl TC, Cunderla B *et al.* Molecular and phenetic characterization of the bacterial assemblage of Hot Lake, WA, an environment with high concentrations of magnesium sulphate, and its relevance to Mars. *Int J Astrobiol* 2014;**13**:69–80.

Klatt CG, Liu Z, Ludwig M *et al.* Temporal metatranscriptomic patterning in phototrophic Chloroflexi inhabiting a microbial mat in a geothermal spring. *ISME J* 2013;**7**:1775–89.

Klatt CG, Wood JM, Rusch DB *et al.* Community ecology of hot spring cyanobacterial mats: predominant populations and their functional potential. *ISME J* 2011;**5**:1262–78.

Kolde R. *pheatmap: Pretty Heatmaps. R package version 1.0. 2*, 2015.

Konopka A, Lindemann S, Fredrickson J. Dynamics in microbial communities: unraveling mechanisms to identify principles. *ISME J* 2015;**9**:1488–95.

Kozich JJ, Westcott SL, Baxter NT *et al.* Development of a dual-index sequencing strategy and curation pipeline for analyzing amplicon sequence data on the MiSeq Illumina sequencing platform. *Appl Environ Microb* 2013;**79**:5112–20.

Kruschel C, Castenholz RW. The effect of solar UV and visible irradiance on the vertical movements of cyanobacteria in microbial mats of hypersaline waters. *FEMS Microbiol Ecol* 1998;**27**:53–72.

Kunin V, Raes J, Harris JK *et al.* Millimeter-scale genetic gradients and community-level molecular convergence in a hypersaline microbial mat. *Mol Syst Biol* 2008;**4**:198.

Langmead B, Salzberg SL. Fast gapped-read alignment with Bowtie 2. *Nat Methods* 2012;**9**:357–9.

Lee JZ, Burow LC, Woebken D *et al.* Fermentation couples Chloroflexi and sulfate-reducing bacteria to Cyanobacteria in hypersaline microbial mats. *Front Microbiol* 2014;**5**:61.

Leshin L, Mahaffy P, Webster C *et al.* Volatile, isotope, and organic analysis of martian fines with the Mars Curiosity rover. *Science* 2013;**341**:1238937.

Lewandowski Z, Beyenal H. *Fundamentals of Biofilm Research*. Boca Raton, FL: CRC Press, 2013.

Ley RE, Harris JK, Wilcox J *et al.* Unexpected diversity and complexity of the Guerrero Negro hypersaline microbial mat. *Appl Environ Microb* 2006;**72**:3685–95.

Lindemann SR, Bernstein HC, Song H-S *et al.* Engineering microbial consortia for controllable outputs. *ISME J* 2016;**10**:2077–84.

Lindemann SR, Moran JJ, Stegen JC *et al.* The epsomitic phototrophic microbial mat of Hot Lake, Washington: community structural responses to seasonal cycling. *Front Microbiol* 2013;**4**:323.

López-López A, Richter M, Peña A *et al.* New insights into the archaeal diversity of a hypersaline microbial mat obtained by a metagenomic approach. *Syst Appl Microbiol* 2013;**36**:205–14.

McMurdie PJ, Holmes S. phyloseq: an R package for reproducible interactive analysis and graphics of microbiome census data. *PLoS One* 2013;**8**:e61217.

Mobberley J, Khodadad C, Visscher P *et al.* Inner workings of thrombolites: spatial gradients of metabolic activity as revealed by metatranscriptome profiling. *Sci Rep* 2015;**5**:12601. doi:10.1038/srep12601.

Moran JJ, Doll CG, Bernstein HC *et al.* Spatially tracking 13C-labelled substrate (bicarbonate) accumulation in microbial communities using laser ablation isotope ratio mass spectrometry. *Environ Microbiol Rep* 2014;**6**:786–91.

Morris RL, Schmidt TM. Shallow breathing: bacterial life at low O2. *Nat Rev Microbiol* 2013;**11**:205–12.

Müller AL, Kjeldsen KU, Rattei T *et al.* Phylogenetic and environmental diversity of DsrAB-type dissimilatory (bi) sulfite reductases. *ISME J* 2015;**9**:1152–65.

Oksanen J, Blanchet FG, Kindt R *et al. Package 'vegan'. Community Ecology Package, R package version 2.3-5*. 2013.

Oren A. Industrial and environmental applications of halophilic microorganisms. *Environ Technol* 2010;**31**:825–34.

Oren A. Thermodynamic limits to microbial life at high salt concentrations. *Environ Microbiol* 2011;**13**:1908–23.

Orphan V, Jahnke L, Embaye T *et al.* Characterization and spatial distribution of methanogens and methanogenic biosignatures in hypersaline microbial mats of Baja California. *Geobiology* 2008;**6**:376–93.

Parks DH, Imelfort M, Skennerton CT *et al.* CheckM: assessing the quality of microbial genomes recovered from isolates, single cells, and metagenomes. *Genome Res* 2015;**25**:1043–55.

Peng Y, Leung HC, Yiu S-M *et al.* IDBA-UD: a de novo assembler for single-cell and metagenomic sequencing data with highly uneven depth. *Bioinformatics* 2012;**28**:1420–8.

Pruesse E, Peplies J, Glöckner FO. SINA: accurate high-throughput multiple sequence alignment of ribosomal RNA genes. *Bioinformatics* 2012;**28**:1823–9.

Rice P, Longden I, Bleasby A. EMBOSS: The European molecular biology open software suite. *Trends Genet* 2000;**16**:276–7.

Rinke C, Schwientek P, Sczyrba A *et al.* Insights into the phylogeny and coding potential of microbial dark matter. *Nature* 2013;**499**:431–7.

Ruvindy R, White RA, III, Neilan BA *et al.* Unravelling core microbial metabolisms in the hypersaline microbial mats of Shark Bay using high-throughput metagenomics. *ISME J* 2016;**10**:183–96.

Stolper DA, Revsbech NP, Canfield DE. Aerobic growth at nanomolar oxygen concentrations. *P Natl Acad Sci USA* 2010;**107**:18755–60.

Strohm TO, Griffin B, Zumft WG *et al.* Growth yields in bacterial denitrification and nitrate ammonification. *Appl Environ Microb* 2007;**73**:1420–4.

Stuart RK, Mayali X, Lee JZ *et al.* Cyanobacterial reuse of extracellular organic carbon in microbial mats. *ISME J* 2015;**10**:1240–51.

Tabita FR, Hanson TE, Li H *et al.* Function, structure, and evolution of the RubisCO-like proteins and their RubisCO homologs. *Microbiol Mol Biol R* 2007;**71**:576–99.

Visscher PT, Stolz JF. Microbial mats as bioreactors: populations, processes, and products. *Palaeogeogr Palaeocl* 2005;**219**:87–100.

Warden JG, Casaburi G, Omelon CR *et al.* Characterization of microbial mat microbiomes in the modern thrombolite ecosystem of Lake Clifton, Western Australia using shotgun metagenomics. *Front Microbiol* 2016;**7**:1064. doi: 10.3389/fmicb.2016.01064.

Wilde A, Mullineaux CW. Motility in cyanobacteria: polysaccharide tracks and type IV pilus motors. *Mol Microbiol* 2015;**98**:998–1001.

Wong HL, Ahmed-Cox A, Burns BP. Molecular ecology of hypersaline microbial mats: current insights and new directions. *Microorganisms* 2016;**4**:6.

Wong HL, Smith D-L, Visscher PT *et al.* Niche differentiation of bacterial communities at a millimeter scale in Shark Bay microbial mats. *Sci Rep* 2015;**5**:15607.

Wu M, Scott AJ. Phylogenomic analysis of bacterial and archaeal sequences with AMPHORA2. *Bioinformatics* 2012;**28**:1033–4.

Yamazaki S, Nomata J, Fujita Y. Differential operation of dual protochlorophyllide reductases for chlorophyll biosynthesis in response to environmental oxygen levels in the cyanobacterium Leptolyngbya boryana. *Plant Physiol* 2006;**142**:911–22.

Yin Y, Mao X, Yang J *et al.* dbCAN: a web resource for automated carbohydrate-active enzyme annotation. *Nucleic Acids Res* 2012;**40**:W445–51.

Yoon S, Cruz-García C, Sanford R *et al.* Denitrification versus respiratory ammonification: environmental controls of two competing dissimilatory NO3−/NO2− reduction pathways in Shewanella loihica strain PV-4. *ISME J* 2015;**9**:1093–104.

Zachara JM, Moran JJ, Resch CT *et al.* Geo-and biogeochemical processes in a heliothermal hypersaline lake. *Geochim Cosmochim Acta* 2016;**181**:144–63.

Zarzycki J, Brecht V, Müller M *et al.* Identifying the missing steps of the autotrophic 3-hydroxypropionate CO2 fixation cycle in Chloroflexus aurantiacus. *PNatl Acad Sci USA* 2009;**106**:21317–22.